VARIOUS MORPHOLOGIES AND SURFACE PROPERTIES OF ANODIZED Zr SURFACES

Ramona RADU[1], Andrei Bogdan STOIAN[2]

Due to their better mechanical properties, metallic biomaterials remain an important choice in dental restorative works and orthopedic surgery. Self-passivation of valve metals such as Ti or Zr is not enough for protection and surface modification is one the ways to improve their performances. The aim of this study is to compare surface morphology, chemistry and physical properties of nanostructured Zr obtained electrochemically at 30 and 60 V using a mixture of H_3PO_4 and NaF aqueous solution as electrolyte.

Keywords: anodizing, SEM, surface properties, AFM, electrochemical test.

1. Introduction

Despite the development and extended use of ceramic and polymeric biomaterials, metals due to their better mechanical properties remain an important choice in dental restorative works and orthopedic surgery [1]. Both Ti and Zr are biocompatible metals with high resistance to corrosion in many aggressive media including bioliquids due to the existence of a native passive film on their surfaces [2, 3]. It is well known that Zr is covered with a ZrO_2 (zirconia) native passive film on the surface which has better osseointegration when compared to Ti [3] and in the oral cavity, it is not affected by plaque accumulation [3]. Self-passivation of Ti or Zr is, however, not enough for protection, so surface modifications are usually employed to improve their performances [4, 5].

We can mention as surface modifications the hydrothermal treatment [5], anodic oxidation [6], acid-etching [7], alkali and heat treatment [8], electrochemical deposition [9] and sol gel preparation [10].

Due to the high surface/volume ratio of nanoarhitectures, processing surfaces at nanolevel is a short way to enhance mechanical, electrochemical stability, bioactivity and bone cell attachment [11]. Anodizing is a very used processing method and the mechanism of self-organized layers of ZrO_2 nanostructures grown by anodizing is closely related to other valve metals [12-14], being a competition between oxide formation and dissolution after fluoride penetration. Anodizing has the advantage of a very flexible procedure and the

[1] PhD student, Dept. of General Chemistry, University POLITEHNICA of Bucharest, Romania
[2*] PhD in Chemistry, Dept. of General Chemistry, University POLITEHNICA of Bucharest, Romania, *coresponding author e-mail: andreibstoian@yahoo.com

nanoarhitecture fabrication by such method on valve metals such as Zr and Ti is controlled by electrolyte composition, pH, temperature and applied voltage.

Various kinds of annealing after anodizing including flame [15] or oxygen absence [16] leading to different oxide properties were investigated. The effect of anodizing parameters on the surface characteristics and electrochemical behavior of Zr has multiple aspects and despite the need of investigations in the context of extended use of Zr in oral cavity and in electronics there are few papers on this topics [14, 17].

The goal of the present manuscript is to compare surface morphology, chemistry and physical properties of nanostructured Zr obtained electrochemically at 30 V and 60 V using a mixture of H_3PO_4 + NaF as aqueous electrolyte. The surface AFM measurements at various distances permitted adhesion forces evaluations and represent the novelty of the manuscript.

2. Experimental part

2.1. Materials and methods

The Zr samples (Sigma Aldrich flat foils, thickness 0.1 mm) were cut to the dimensions 5×1 cm, then washed with ethylic alcohol and water (10 minutes each). Anodizing was performed for 60 minutes at 30 V and 60 V using a Pt cathode. The anodizing electrolyte was prepared as follows: 5 mL of 85% H_3PO_4 solution were diluted with 45 mL of distilled water, then 0.07 grams of NaF salt were added and solution was mixed for 5 minutes.

2.2. Surface characterization

Surface characterization of samples included scanning electron microscopy (SEM), atomic force microscopy (AFM) and contact angle determinations. SEM was performed with a Quantum 650 FEG microscope applying 5 kV in high vacuum. In order to analyze the phase formation of ZrO_2, X-ray diffraction (XRD) was performed with a Shimadzu XRD 6000 equipment with Cu K radiation (λ = 1.5406 Å). Micro roughness and adhesion forces were evaluated using an A.P.E. Research A100-SGS AFM microscope. The contact angle equipment for evaluation of hydrophilic-hydrophobic balance was CAM 100 using distilled water. The film-substrate bond strength was evaluated from film detachment experiments carried out with a PosiTest AT-M adhesion tester from DeFelsko using 1 cm diameter aluminium dollies.

2.3. Electrochemical tests

The electrochemical tests were performed using an Autolab PGSTAT 302N equipment for ZrO_2 samples immersed in Afnor artificial saliva with composition presented in Table 1. A conventional three electrode system with Zr samples as the working electrode, Pt foil as the counter electrode and a Ag/AgCl reference electrode was used for recording the potentiodynamic polarization

curves. Before each measurement, the potential was left to stabilize for 10 min at open circuit. Polarization data were registered between ±200 mV and free potential (OCP) using a scan rate of 0.2 mV/s at room temperature. Values of corrosion parameters (corrosion potential, corrosion current, corrosion rate and polarization resistance) were evaluated by using Nova 1.10 software. Porosity was also evaluated from values of polarization resistance.

Table 1

Afnor artificial saliva composition [18]

Dissolved salts	NaCl	KCl	Na_2HPO_4	$NaHCO_3$	KSCN	CH_4ON_2
Concentration (g/L)	0.7	1.2	0.26	1.5	0.33	1.33

3. Results and discussion

3.1. Surface characterization

In Fig. 1 the SEM image obtained for the untreated Zr sample shows some fine scratches and naturally formed ZrO_2 with irregular morphologies, the more well-defined grains having diameters ranging from approximately 200 nm to approximately 3 μm.

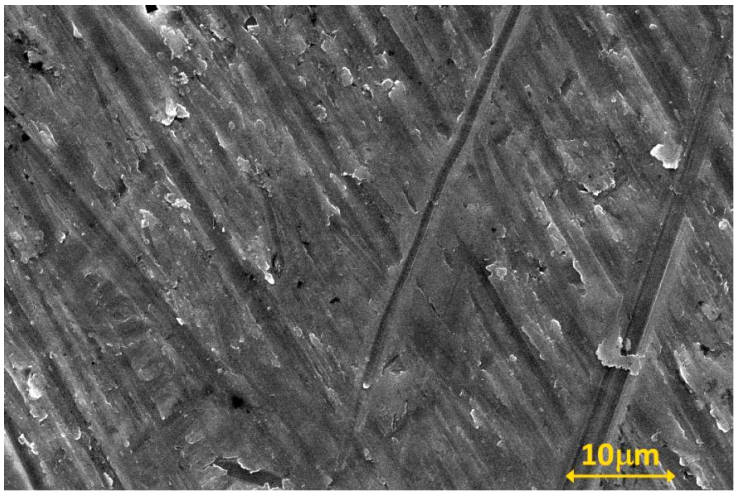

Fig. 1. SEM micrography for untreated Zr (covered naturally with ZrO_2)

On the surface of the sample anodized at 30 V (Fig. 2) there are compact ZrO_2 coated areas, as well as nanoporous areas with diameters of about 50 nm. Under the compact oxide layer and under nanopores there is another layer of nanoporous ZrO_2 with pore diameters ranging from 36.4 nm to 94.6 nm.

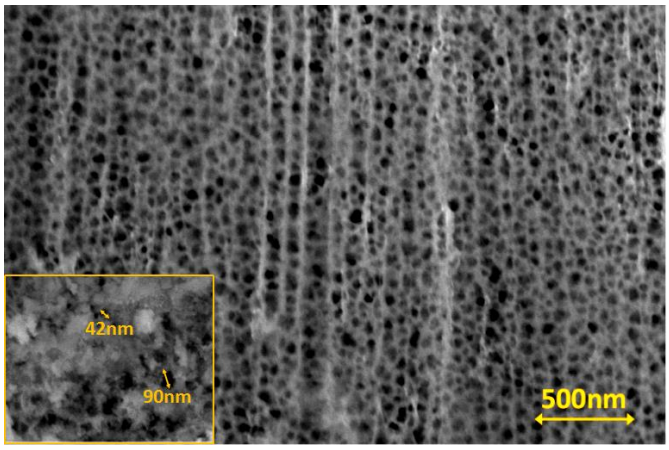

Fig. 2. SEM micrography for Zr anodized at 30 V; inset: ZrO_2 nanoporous under-layer (not to scale)

On the sample anodized at 60 V (Fig. 3) there were observed pores with dimensions between approximately 100 and 500 nm.

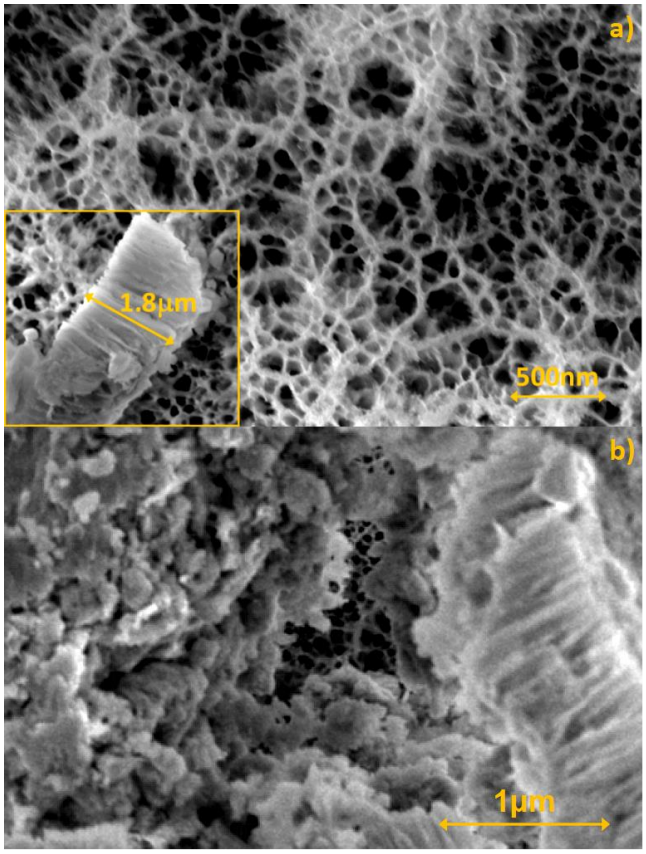

Fig. 3. SEM micrography for Zr anodized at 60 V; a) surface morphology - inset: ZrO_2 nanotubes (not to scale); b) section view showing granular ZrO_2

Under the pore layer (Fig. 3 inset) there is a layer of ZrO_2 nanotubes with a diameter of about 100 nm and lengths of about 1.8 μm. The sample was scratched in order to verify the lengths of the nanotubes. Under the nanotubes there was found another layer of unorganized granular ZrO_2 with grain diameters between approximately 40 and 380 nm. Different studies regarding anodizing Zr in H_3PO_4 [19, 20] have shown that this process produces compact ZrO_2 with some incorporated phosphate compounds in the monoclinic zirconia film. Being a valve metal, the mechanism of ZrO_2 nanopores and nanotubes formation by anodizing is related to that of TiO_2 nanotubes, flouride ions presence in the electrolyte and the formation and dissolution of Zr fluoro-complexes being essential parts of the process. However, small variations occurring during the preparations of the samples, anodizing conditions or even environmental changes can disturb the fine balance of anodic oxide formation, Zr fluoro-complex formation and dissolution, leading to different results for seemingly identical conditions [21]. One study [22] confirms the formation of unorganized granular ZrO_2 under the formed nanotubes at higher positive potentials.

XRD diffraction patterns (Fig. 4) matched with JCPDS 14-0534 and JCPDS 37-1484 reveal that there is a mixture of monoclinic (m-ZrO_2) and tetragonal (t-ZrO_2) crystaline phases on the surface of the samples. The distinguished characteristic peaks for m-ZrO_2 and t-ZrO_2 appear at the same 2θ values but differ in intensity.

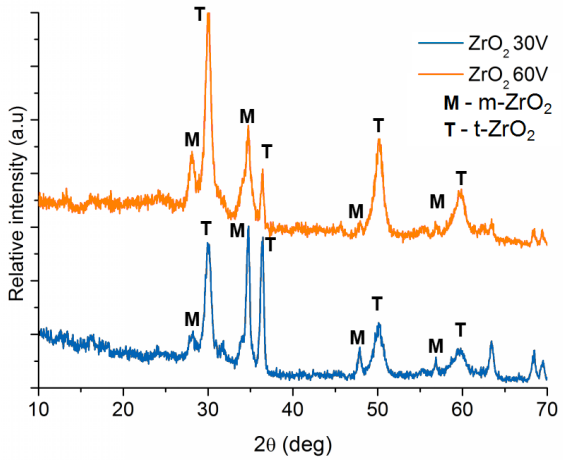

Fig. 4. XRD pattern for anodized Zr

The intensities of some peaks attributed to t-ZrO_2 (2θ = 30.2, 36.7, 50.2 and 60.2°) on the sample obtained at 60 V are larger than those recorded on the sample obtained at 30 V. The peaks attributed to m-ZrO_2 were found at 2θ = 28, 34.7, 48 and 56.3°. No notable differences were observed for the peaks attributed to m-ZrO_2 for the two samples, however there are small variations in angle values when compared to other papers [23, 24]. The presence of phosphate compounds

could not be validated, the main peaks at 2θ = 11.9, 19.8 and 25° being absent [25].

The nano crystallite size was calculated using the Scherrer equation:

$$D = K\lambda / \beta \cdot \cos\theta \quad (1)$$

where λ is the X-ray wavelength in nanometers (nm), β is the peak width of the diffraction peak profile at half maximum height resulting from small crystallite size in radians and K is a constant related to crystallite shape, normally taken as 0.9, θ is the incidence angle of the x-ray beam. [26].

The average calculated crystallite sizes obtained from the main four evidenced XRD peaks are presented in Table 2. They are smaller to those reported by others, but differences occur when using different techniques for obtaining ZrO_2 [26, 27].

Table 2

Nano crystallite size for analyzed samples

Sample	m-ZrO_2 average size (nm)	t-ZrO_2 average size (nm)
ZrO_2 30 V	21.70	9.81
ZrO_2 60 V	28.65	8.66

The studied surface properties values were presented in a scheme (Fig. 5) which enables a correlation between the samples. Contact angle determinations reveal that anodizing produces a strong increase of the hydrophilic character of the samples (values of 10-12°). As a surface becomes more oxidized, or has more ionizable groups introduced to it, hydrogen bonding with the water becomes more facile and the droplet spreads along the hydrophilic surface, resulting in a lower contact angle [28]. Also, contact angle values are also dependent on the topography of the sample. Water molecules can penetrate through capillary forces the pores of the material and wet the surface completely.

The adhesion forces measured by AFM are showing an overall decreasing trend and can be correlated very well with the contact angle values. It seems that superhydrophilic samples hinder the formation of the water interface between the sample and the AFM cantilever, thus giving small adhesion forces.

Inversely proportional to both contact angle values and adhesion forces are other properties such as the roughness and film delamination forces. Roughness values (Ra) of anodized Zr samples are two times greater than natural ZrO_2, whereas values of delamination forces increase with around 50%. The increase of roughness, also observed by others in anodized Zr [29] and film delamination forces, were attributed to the existence of new ZrO_2 structures on the surface that make the samples more uneven but act as enhanced binders on the metallic Zr substrate. Although AFM adhesion force measurements were reported for ZrO_2 [30], the literature is scarce, and to the best of our knowledge, the correlation

between AFM adhesion forces at nano level and film delamination forces at macro level, was never reported before.

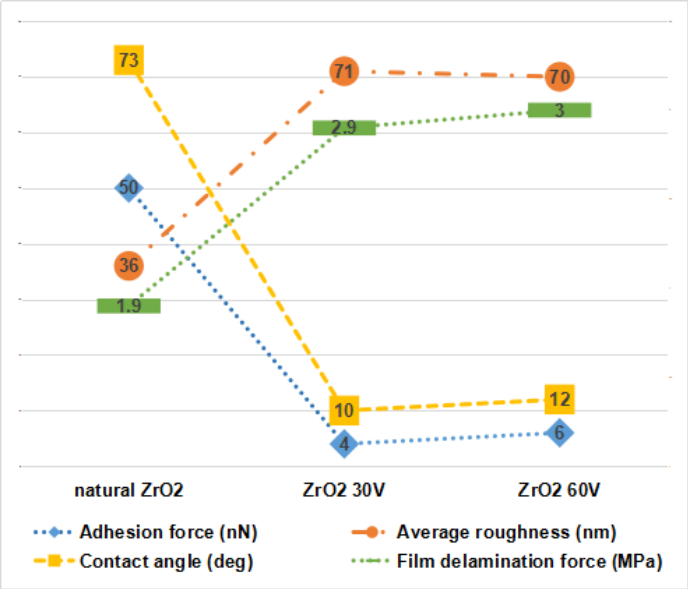

Fig. 5. Correlated surface properties for studied samples

3.2. Electrochemical tests

The polarization data in Afnor artificial saliva are represented as potentiodynamic polarization curves (Fig. 6) and the obtained corrosion parameters are listed in Table 2.

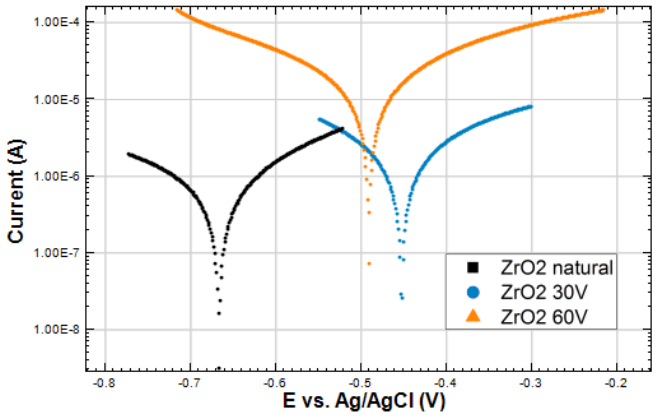

Fig. 6. Tafel plots recorded for analysed ZrO_2 samples

The corrosion potential for sample anodized at 30 V shifts positively with 215 mV, thus indicating a very compact passive layer of ZrO_2. On contrary, anodization at 60 V has produced a smaller shift of E_{corr}, indicating a less compact

oxide layer. Unexpectedly, the obtained data for polarized samples indicate that the corrosion rate increases and polarization resistance decreases, respectively, with the anodizing potential.

Table 2

Polarization data of analysed samples

Sample	E_{corr} (mV)	I_{corr} (μA)	Corrosion rate (mm/y)	Polarization resistance (kΩ)	Porosity (%)	βa (mV/dec)
Zr (natural ZrO_2)	-667	1.69	0.0042	49.51	-	528
ZrO_2 30 V	-452	6.47	0.0335	18.64	22.18	516
ZrO_2 60 V	-493	14.98	0.0770	3.40	37.67	234

This behavior can be explained by the different morphologies of the samples themselves. The naturally formed oxide, although is a thin film, is fairly uniform, whereas by anodization many pores and nanotubes appear, drasticaly increasing the surface of the samples. This means that a lot more area of the samples is being subjected to the corrosive environment. Since the surface is not homogenous, we were not able to calculate the real area of the surface. From the polarization resistance data (Table 2) we calculated the porosities of the samples using the equation (2) [31]:

$$P = [(Rp_{substrate}/Rp_{anodized}) \cdot 10^{-(|\Delta E|/\beta\alpha)}] \cdot 100\% \quad (2)$$

where $Rp_{substrate}$ is the polarization resistance of the substrate before anodizing, $Rp_{anodized}$ is the polarization resistance of the anodized sample, $\Delta E|$ is the difference between the substrate and anodized surface corrosion potentials and βa is the anodic Tafel slope for the substrate curve. The calculated porosity values are in accordance with qualitative comparison of SEM images revealing that the most porous surface was obtained at 60 V.

6. Conclusions

Zr samples were anodized at 30 V and 60 V in a mixture of H_3PO_4 + NaF dissolved in water, then compared in terms of surface properties and electrochemical behaviour with naturally oxidized Zr. The morphologies of the anodized samples differ, since at 30 V only small nanopores form and at 60 V larger nanopores and nanotubes were formed. The cristalinity of the samples was affected to a lesser extent by the anodizing potential, both samples being covered by a mixture of monoclinic and tetragonal ZrO_2. The AFM determined adhesion force and contact angle decrease with the increase of the anodizing potential, whereas the roughness and film delaminatiion forces increase with the increase of the potential. From the electrochemical tests made in Afnor artificial saliva we

can conclude that anodizing of zirconium produces samples with greatly increased areas.

Acknowledgments

This work was supported by CNCSIS–UEFISCSU, project number PN-III-P4-ID PCE 2016-0316.

R E F E R E N C E S

[1]. *M. McCracken*, "Dental implant materials: Commercially pure titanium and titanium alloys", J. Prosthod., **vol. 8**, no. 1, 1999, pp. 40-43

[2]. *M. V. Popa, I. Demetrescu, D. Iordachescu, A. Cimpan, E. Vasilescu, P. Drob, D. Ionita, C. Vasilescu, M. Istratescu*, "The relation between electrochemical test and in vitro evaluation of titanium alloy biocompatibility", Materials and Corrosion, **vol. 58**, no. 9, 2007, pp. 667-675

[3]. *N. Bernhard, S. Berner, M. de Wild, M. Wieland*, "The binary TiZr alloy - A newly developed Ti alloy for use in dental implants", Forum Implantologicum, **vol. 5**, 2009, pp. 30-39

[4]. *A. Mazare, G. Totea, C. Burnei, P. Schmuki, I. Demetrescu, D. Ionita*, "Corrosion, antibacterial activity and haemocompatibility of TiO_2 nanotubes as a function of their annealing temperature", Corrosion Science, **vol. 103**, 2016, pp. 215-222

[5]. *T. Hanawa*, "Biofunctionalization of titanium for dental implant", Japanese Dental Science Review, **vol. 46**, no. 2, 2010, pp. 93-101

[6]. *D. Portan, D. Ionita, I. Demetrescu*, "Monitoring TiO_2 nanotubes elaboration condition, a way for obtaining various characteristics of nanostructures", Key Engineering Materials, **vol. 415**, 2009, pp. 9-12

[7]. *A. Jemat, M. J. Ghazali, M. Razali, Y. Otsuka*, "Surface modifications and their effects on titanium dental implants", BioMed Research International, **vol. 2015**, 2015, ID 791725

[8]. *I. Hamouda, E. Enan, E. Al Wakeel, M. Yousef*, "Alkali and heat treatment of titanium implant material for bioactivity", The International Journal of Oral & Maxillofacial Implants, **vol. 27**, 2012, pp. 776-84.

[9]. *M. Vardaki, M. Prodana, A. B. Stoian, D. Ionita*, "Corrosion and bioactivity of a bioinspired coating on TiZr alloys U.P.B. Sci. Bull., Series B, **vol. 80**, no. 1, 2018

[10]. *D. Ionita, M.Vardaki, M. S. Stan, A. Dinischiotu, I. Demetrescu*, "Enhance stability and in vitro cell response to a bioinspired coating on Zr alloy with increasing chitosan content", Journal of Bionic Engineering, **vol. 14**, no.3, 2017, pp. 459-467

[11]. *S. Minagar, C. Berndt, T. Gengenbach, C. Wen*, "Fabrication and characterization of TiO_2–ZrO_2–$ZrTiO_4$ nanotubes on TiZr alloy manufactured via anodization' Journal of Materials Chemistry B, **vol. 2**, 2013, pp. 71-83

[12]. *H. Tsuchiya, P. Schmuki*, "Thick self-organized porous zirconium oxide formed in H2SO4/NH4F electrolytes", Electrochemistry Communications, **vol. 6**, no. 11, 2004, pp. 1131-1134

[13]. *S. Ismail, Z. A. Ahmad, A. Berenov, Z. Lockman*, "Effect of applied voltage and fluoride ion content on the formation of zirconia nanotube arrays by anodic oxidation of zirconium", Corrosion Science, **vol. 53**, no. 4, 2011, pp. 1156-1164

[14]. *A. Gomez Sanchez, W. Schreiner, G. Duffó, S. Ceré*, "Surface characterization of anodized zirconium for biomedical applications", Applied Surface Science, **vol. 257**, no. 15, 2011, pp. 6397-6405

[15]. *A. Mazare, I. Paramasivam, F. Schmidt-Stein, K. Lee, I. Demetrescu, P. Schmuki*, "Flame annealing effects on self-organized TiO_2 nanotubes", Electrochimica Acta, **vol. 66**, 2012, pp. 12-21

[16]. *A. Ghicov, H. Tsuchiya, J.M. Macak, P. Schmuki*, "Annealing effects on the photoresponse of TiO_2 nanotubes", Physica Status Solidi (A) Applications and Materials Science, **vol. 203**, no. 4, 2006, pp. R28-R30 2006

[17]. *D.E. Romonti, A. V. Gomez Sanchez, I. Milošev, I. Demetrescu, S. Ceré*, "Effect of anodization on the surface characteristics and electrochemical behaviour of zirconium in artificial saliva", Materials Science and Engineering: C, **vol. 62**, 2016, pp. 458-466

[18]. *E. Aldea, A. Meghea, I. Demetrescu*, "Comparison of the antioxidant activity of various simulated artificial saliva", Proceedings of the International Semiconductor Conference, CAS, **vol. 2**, 2003, pp. 331-334

[19]. *M. R Katunar, A. Gomez Sanchez, A. S. Coquillat, A. Civantos, E. M. Campos, J. Ballarre, T. Vicoa, M, Baca, V. Ramos, S. Cere*, "In vitro and in vivo characterization of anodised zirconium as a potential material for biomedical applications", Materials Science and Engineering C, **vol. 75**, 2017, pp. 957–968

[20]. *A. Gomez Sanchez, W. Schreiner, G. Duffó, S. Ceré*, "Surface characterization of anodized zirconium for biomedical applications", Applied Surface Science, **vol. 257**, 2011, pp. 6397–6405

[21]. *D. E. Romonti, A. V. Gomez Sanchez, I. Milošev, I.Demetrescu, S. Ceré*, "Effect of anodization on the surface characteristics and electrochemical behaviour of zirconium in artificial saliva', Materials Science and Engineering C, **vol. 62**, 2016, pp. 458–466

[22]. *S. Ismail, Z. A. Ahmad, A. Berenov, Z. Lockman*, "Effect of applied voltage and fluoride ion content on the formation of zirconia nanotube arrays by anodic oxidation of zirconium", Corrosion Science, **vol. 53**, 2011, pp. 1156-1164

[23]. *M. Gauna, S. Conconi, S. Gómez, G. Suarez, E. F. Aglietti, N. Rendtorff*, "Monoclinic-tetragonal zirconia quantification of commercial nanopowder mixtures by XRD and DTA", Ceramics Silikaty, **vol. 59**, 2015, pp. 318-325

[24]. *Z. Xu, Y. Zheng, Y. Guo, W. Ye, P. Yang*, "Microstructure evolution and model analysis of Al_2O_3/ZrO_2 hypoeutectic ceramic during rapid solidification", Materials Research, **vol. 18**, 2015, pp. 146-151

[25]. *G. García-Rosales, O. Regil Enrique, E. Romero Guzman, E. Teresita, E. Ordonez-Regil*, "The influence of agitation speed on the morphology and size particle synthesis of $Zr(HPO_4)_2{\cdot}H_2O$ from mexican sand, Journal of Minerals and Materials Characterization and Engineering, **vol. 6**, 2007, pp. 39-51

[26]. *S. Jayakumar, P.V. Ananthapadmanabhan, K. Perumal, T.K. Thiyagarajan, S.C. Mishra, L.T. Su, A.I.Y. Tok, J. Guo*, "Characterization of nano-crystalline ZrO_2 synthesized via reactive plasma processing", Materials Science and Engineering: B, **vol. 176**, 2011, pp. 894-899

[27]. *M. Bashir, I. Abbas, S. Riaz, Y.-J. Guo, S. Naseem*, "Structural, morphological and mechanical properties of zirconia nanostructures for bone implantations", Conference: The 2016 World Congress on Advances in Civil, Environmental and Materials Research (ACEM'16), Korea

[28]. *C.-C. Wu, C.-K. Wei, C.-C. Ho, S.-J. Ding*, "Enhanced hydrophilicity and biocompatibility of dental zirconia ceramics by oxygen plasma treatment", Materials, **vol. 8**, 2015, pp. 684-699

[29]. *F. Vacandioz, M. Eyraud, C. Chassigneux, P. Knauth, T. Djenizian*, "Electrochemical synthesis and characterization of zirconia nanotubes grown from Zr thin films", Journal of The Electrochemical Society, **vol. 157**, 2010, pp. K279-K283

[30]. *N. Zaouri, L. Gutierrez, L. Dramas, D. Garces, J.-P. Croue*, "Interfacial interactions between Skeletonema costatum extracellular organic matter and metal oxides: Implications for ceramic membrane filtration", Water Research, **vol. 116**, 2017, pp. 194-202

[31]. *J. F. Flores, J. J. Olaya, R. Colás, S. E. Rodil, B. S. Valdez, I. G. Fuente*, "Corrosion behaviour of TaN thin PVD films on steels", Corrosion Engineering, Science and Technology, **vol. 41**, pp. 168-176.